EUROPEAN ORGANISATION FOR NUCLEAR RESEARCH

CERN-PPE/95-027
13 March 1995

Inclusive strange vector and tensor meson production in hadronic Z^0 decays

The OPAL Collaboration

Abstract

Measurements have been made in the OPAL experiment at LEP of the inclusive production of strange vector $\phi(1020)$ and $K^*(892)^0$ mesons, and the tensor meson $K_2^*(1430)^0$. The overall production rates per hadronic Z^0 decay have been determined to be $0.100 \pm 0.004 \pm 0.007$ $\phi(1020)$ mesons, $0.74 \pm 0.03 \pm 0.03$ $K^*(892)^0$ mesons and (for $x_E < 0.3$) $0.19 \pm 0.04 \pm 0.06$ $K_2^*(1430)^0$ mesons. The measurements for the vector states update previously published results based on lower statistics, while the $K_2^*(1430)^0$ rate represents the first direct measurement of a strange tensor state in Z^0 decay. For the vector states, both the overall production rates and normalised differential cross sections, with respect to the scaled energy variable x_E, have been compared to JETSET and HERWIG predictions. The peak positions in the $\xi = \ln(1/x_p)$ distributions have been measured and found to be consistent with measurements of other hadron states.

(to be submitted to Zeitschrift für Physik C)

The OPAL Collaboration

R. Akers[16], G. Alexander[23], J. Allison[16], K. Ametewee[25], K.J. Anderson[9], S. Arcelli[2], S. Asai[24], D. Axen[29], G. Azuelos[18,a], A.H. Ball[17], E. Barberio[26], R.J. Barlow[16], R. Bartoldus[3], J.R. Batley[5], G. Beaudoin[18], A. Beck[23], G.A. Beck[13], C. Beeston[16], T. Behnke[27], K.W. Bell[20], G. Bella[23], S. Bentvelsen[8], P. Berlich[10], S. Bethke[14], O. Biebel[14], I.J. Bloodworth[1], P. Bock[11], H.M. Bosch[11], M. Boutemeur[18], S. Braibant[12], P. Bright-Thomas[25], R.M. Brown[20], A. Buijs[8], H.J. Burckhart[8], R. Bürgin[10], C. Burgard[27], N. Capdevielle[18], P. Capiluppi[2], R.K. Carnegie[6], A.A. Carter[13], J.R. Carter[5], C.Y. Chang[17], C. Charlesworth[6], D.G. Charlton[1,b], S.L. Chu[4], P.E.L. Clarke[15], J.C. Clayton[1], S.G. Clowes[16], I. Cohen[23], J.E. Conboy[15], O.C. Cooke[16], M. Cuffiani[2], S. Dado[22], C. Dallapiccola[17], G.M. Dallavalle[2], C. Darling[31], S. De Jong[12], L.A. del Pozo[8], H. Deng[17], M. Dittmar[4], M.S. Dixit[7], E. do Couto e Silva[12], J.E. Duboscq[8], E. Duchovni[26], G. Duckeck[8], I.P. Duerdoth[16], U.C. Dunwoody[5], J.E.G. Edwards[16], P.A. Elcombe[5], P.G. Estabrooks[6], E. Etzion[23], H.G. Evans[9], F. Fabbri[2], B. Fabbro[21], M. Fanti[2], P. Fath[11], M. Fierro[2], M. Fincke-Keeler[28], H.M. Fischer[3], P. Fischer[3], R. Folman[26], D.G. Fong[17], M. Foucher[17], H. Fukui[24], A. Fürtjes[8], P. Gagnon[6], A. Gaidot[21], J.W. Gary[4], J. Gascon[18], N.I. Geddes[20], C. Geich-Gimbel[3], S.W. Gensler[9], F.X. Gentit[21], T. Geralis[20], G. Giacomelli[2], P. Giacomelli[4], R. Giacomelli[2], V. Gibson[5], W.R. Gibson[13], J.D. Gillies[20], J. Goldberg[22], D.M. Gingrich[30,a], M.J. Goodrick[5], W. Gorn[4], C. Grandi[2], E. Gross[26], J. Hagemann[27], G.G. Hanson[12], M. Hansroul[8], C.K. Hargrove[7], P.A. Hart[9], M. Hauschild[8], C.M. Hawkes[8], E. Heflin[4], R.J. Hemingway[6], G. Herten[10], R.D. Heuer[8], J.C. Hill[5], S.J. Hillier[8], T. Hilse[10], P.R. Hobson[25], D. Hochman[26], R.J. Homer[1], A.K. Honma[28,a], R. Howard[29], R.E. Hughes-Jones[16], P. Igo-Kemenes[11], D.C. Imrie[25], A. Jawahery[17], P.W. Jeffreys[20], H. Jeremie[18], M. Jimack[1], M. Jones[6], R.W.L. Jones[8], P. Jovanovic[1], C. Jui[4], D. Karlen[6], J. Kanzaki[24], K. Kawagoe[24], T. Kawamoto[24], R.K. Keeler[28], R.G. Kellogg[17], B.W. Kennedy[20], B. King[8], J. King[13], J. Kirk[29], S. Kluth[5], T. Kobayashi[24], M. Kobel[10], D.S. Koetke[6], T.P. Kokott[3], S. Komamiya[24], R. Kowalewski[8], T. Kress[11], P. Krieger[6], J. von Krogh[11], P. Kyberd[13], G.D. Lafferty[16], H. Lafoux[8], R. Lahmann[17], W.P. Lai[19], J. Lauber[8], J.G. Layter[4], P. Leblanc[18], A.M. Lee[31], E. Lefebvre[18], D. Lellouch[26], C. Leroy[18], J. Letts[2], L. Levinson[26], S.L. Lloyd[13], F.K. Loebinger[16], G.D. Long[17], B. Lorazo[18], M.J. Losty[7], X.C. Lou[8], J. Ludwig[10], A. Luig[10], M. Mannelli[8], S. Marcellini[2], C. Markus[3], A.J. Martin[13], J.P. Martin[18], T. Mashimo[24], W. Matthews[25], P. Mättig[3], U. Maur[3], J. McKenna[29], T.J. McMahon[1], A.I. McNab[13], F. Meijers[8], F.S. Merritt[9], H. Mes[7], A. Michelini[8], R.P. Middleton[20], G. Mikenberg[26], D.J. Miller[15], R. Mir[26], W. Mohr[10], A. Montanari[2], T. Mori[24], M. Morii[24], U. Müller[3], B. Nellen[3], B. Nijjhar[16], S.W. O'Neale[1], F.G. Oakham[7], F. Odorici[2], H.O. Ogren[12], N.J. Oldershaw[16], C.J. Oram[28,a], M.J. Oreglia[9], S. Orito[24], F. Palmonari[2], J.P. Pansart[21], G.N. Patrick[20], M.J. Pearce[1], P.D. Phillips[16], J.E. Pilcher[9], J. Pinfold[30], D.E. Plane[8], P. Poffenberger[28], B. Poli[2], A. Posthaus[3], T.W. Pritchard[13], H. Przysiezniak[30], M.W. Redmond[8], D.L. Rees[8], D. Rigby[1], M.G. Rison[5], S.A. Robins[13], D. Robinson[5], N. Rodning[30], J.M. Roney[28], E. Ros[8], A.M. Rossi[2], M. Rosvick[28], P. Routenburg[30], Y. Rozen[8], K. Runge[10], O. Runolfsson[8], D.R. Rust[12], M. Sasaki[24], C. Sbarra[2], A.D. Schaile[8], O. Schaile[10], F. Scharf[3], P. Scharff-Hansen[8], P. Schenk[4], B. Schmitt[3], M. Schröder[8], H.C. Schultz-Coulon[10], P. Schütz[3], M. Schulz[8], C. Schwick[27], J. Schwiening[3], W.G. Scott[20], M. Settles[12], T.G. Shears[5], B.C. Shen[4], C.H. Shepherd-Themistocleous[7], P. Sherwood[15], G.P. Siroli[2], A. Skillman[15], A. Skuja[17], A.M. Smith[8], T.J. Smith[28], G.A. Snow[17], R. Sobie[28], S. Söldner-Rembold[10], R.W. Springer[30], M. Sproston[20], A. Stahl[3], M. Starks[12], C. Stegmann[10], K. Stephens[16],

J. Steuerer[28], B. Stockhausen[3], D. Strom[19], P. Szymanski[20], R. Tafirout[18], H. Takeda[24], T. Takeshita[24], P. Taras[18], S. Tarem[26], M. Tecchio[9], P. Teixeira-Dias[11], N. Tesch[3], M.A. Thomson[8], O. Tousignant[18], S. Towers[6], M. Tscheulin[10], T. Tsukamoto[24], A.S. Turcot[9], M.F. Turner-Watson[8], P. Utzat[11], R. Van Kooten[12], G. Vasseur[21], P. Vikas[18], M. Vincter[28], A. Wagner[27], D.L. Wagner[9], C.P. Ward[5], D.R. Ward[5], J.J. Ward[15], P.M. Watkins[1], A.T. Watson[1], N.K. Watson[7], P. Weber[6], P.S. Wells[8], N. Wermes[3], B. Wilkens[10], G.W. Wilson[27], J.A. Wilson[1], V-H. Winterer[10], T. Wlodek[26], G. Wolf[26], S. Wotton[11], T.R. Wyatt[16], A. Yeaman[13], G. Yekutieli[26], M. Yurko[18], V. Zacek[18], W. Zeuner[8], G.T. Zorn[17].

[1]School of Physics and Space Research, University of Birmingham, Birmingham B15 2TT, UK
[2]Dipartimento di Fisica dell' Università di Bologna and INFN, I-40126 Bologna, Italy
[3]Physikalisches Institut, Universität Bonn, D-53115 Bonn, Germany
[4]Department of Physics, University of California, Riverside CA 92521, USA
[5]Cavendish Laboratory, Cambridge CB3 0HE, UK
[6]Carleton University, Department of Physics, Colonel By Drive, Ottawa, Ontario K1S 5B6, Canada
[7]Centre for Research in Particle Physics, Carleton University, Ottawa, Ontario K1S 5B6, Canada
[8]CERN, European Organisation for Particle Physics, CH-1211 Geneva 23, Switzerland
[9]Enrico Fermi Institute and Department of Physics, University of Chicago, Chicago IL 60637, USA
[10]Fakultät für Physik, Albert Ludwigs Universität, D-79104 Freiburg, Germany
[11]Physikalisches Institut, Universität Heidelberg, D-69120 Heidelberg, Germany
[12]Indiana University, Department of Physics, Swain Hall West 117, Bloomington IN 47405, USA
[13]Queen Mary and Westfield College, University of London, London E1 4NS, UK
[14]Technische Hochschule Aachen, III Physikalisches Institut, Sommerfeldstrasse 26-28, D-52056 Aachen, Germany
[15]University College London, London WC1E 6BT, UK
[16]Department of Physics, Schuster Laboratory, The University, Manchester M13 9PL, UK
[17]Department of Physics, University of Maryland, College Park, MD 20742, USA
[18]Laboratoire de Physique Nucléaire, Université de Montréal, Montréal, Quebec H3C 3J7, Canada
[19]University of Oregon, Department of Physics, Eugene OR 97403, USA
[20]Rutherford Appleton Laboratory, Chilton, Didcot, Oxfordshire OX11 0QX, UK
[21]CEA, DAPNIA/SPP, CE-Saclay, F-91191 Gif-sur-Yvette, France
[22]Department of Physics, Technion-Israel Institute of Technology, Haifa 32000, Israel
[23]Department of Physics and Astronomy, Tel Aviv University, Tel Aviv 69978, Israel
[24]International Centre for Elementary Particle Physics and Department of Physics, University of Tokyo, Tokyo 113, and Kobe University, Kobe 657, Japan
[25]Brunel University, Uxbridge, Middlesex UB8 3PH, UK
[26]Particle Physics Department, Weizmann Institute of Science, Rehovot 76100, Israel
[27]Universität Hamburg/DESY, II Institut für Experimental Physik, Notkestrasse 85, D-22607 Hamburg, Germany
[28]University of Victoria, Department of Physics, P O Box 3055, Victoria BC V8W 3P6, Canada
[29]University of British Columbia, Department of Physics, Vancouver BC V6T 1Z1, Canada
[30]University of Alberta, Department of Physics, Edmonton AB T6G 2J1, Canada
[31]Duke University, Dept of Physics, Durham, NC 27708-0305, USA

[a]Also at TRIUMF, Vancouver, Canada V6T 2A3
[b] Royal Society University Research Fellow

1 Introduction

The inclusive production rates for a large number of identified meson and baryon states have now been measured in hadronic Z^0 decays. For mesons containing only light quarks (u, d, s), results have been published for all the pseudoscalar states [1, 2, 3] and all the vector mesons [4, 5, 6, 7] except the $\omega(782)$. However, only one scalar meson, the $f_0(980)$, and one tensor meson, the $f_2(1270)$, have been reported [6, 7].

A number of QCD-based Monte Carlo models exist which allow interpretation of measurements of meson production. In JETSET [8], for example, a number of variable parameters can be tuned to reproduce the observations. The values of these parameters may be interpreted as providing information about the nature of the fragmentation process. Measurements of light mesons, as well as of baryons, in all of the various spin-parity and strangeness states are therefore required to provide a full picture of the parton fragmentation.

In this paper, we present results from a sample of 1.2 million multihadronic Z^0 decays recorded by the OPAL detector at LEP between 1990 and 1992. We give measurements of the production rates of the strange vector $K^*(892)^0$ and $\phi(1020)$ mesons, updating the previous OPAL results [4] and providing a significant improvement in precision. In addition we report the first measurement of the strange tensor $K_2^*(1430)^0$ meson. We reconstruct the K^* mesons in their $K^\pm\pi^\mp$ decay modes, and the $\phi(1020)$ in K^+K^-. For the vector states we study, in addition to the fragmentation functions and overall multiplicities, the dependence of the differential cross sections on the variable $\xi = \ln(1/x_p)$, where x_p is the scaled meson momentum. This allows comparisons to be made with predictions of the modified leading log approximation in QCD, using local parton-hadron duality.

2 Data Selection

The OPAL detector is described fully in reference [9]. For the present analysis only information from the central tracking system was used. This consists of a vertex detector for accurate position measurement near the interaction region, a large jet chamber providing a maximum of 159 individual r-ϕ [1] position and ionisation energy loss ($\mathrm{d}E/\mathrm{d}x$) measurements per track, and an outer layer of z-chambers for the determination of track end points in z. In 1991 a silicon microvertex detector [10] was installed in the experiment around the beam pipe. Position measurements made by this detector were used, when available, in the reconstruction of charged tracks for the analysis. The complete tracking system lies within an axial magnetic field of 0.435 T produced by a solenoidal coil. The two-particle mass resolution typically varies from 5 MeV to 20 MeV depending on the mass and momentum of the reconstructed state. A track with the maximum number of energy loss measurements has a $\mathrm{d}E/\mathrm{d}x$ resolution of 3.5%.

For every charged track in each event of the 1.2 million hadronic Z^0 decays (selected as described in [11]) the following quality cuts were applied. Tracks were required to have at least 20 space point measurements in the jet chamber and a point of closest approach to the interaction point of within 40 cm in z and 5 cm in the r-ϕ plane. The radius of the first measured space point for each track was required to be less than 75 cm. A minimum transverse momentum with respect to the beam axis of 0.15 GeV/c was demanded and only tracks with

[1] A right-handed coordinate system is used by OPAL, where positive z is along the electron beam direction and r and ϕ are the usual cylindrical polar coordinates.

polar angles between 21.6° and 158.4° were included. If at least five tracks passed these cuts then the event was considered for the analysis and tested for energy and momentum balance. The event was rejected if the magnitude of the total reconstructed momentum vector of the selected tracks was greater than 40% of the centre of mass energy, or if the total visible energy summed over all charged tracks (assuming all tracks to be pions) was less than 20% of the total available. For the subsequent inclusive meson analyses, only those tracks with momentum $p > 0.25$ GeV/c, polar angle $|\cos\theta| \leq 0.72$ and which contained z information from the z-chambers were used. After these cuts, 925 453 events were left from the original sample, with an average of 11.54 selected tracks per event.

Approximately one million hadronic events generated by the Monte Carlo program JETSET version 7.3 were used in the analysis. The parameters of the JETSET model had been tuned [12] so that the program reproduced many global features of multihadronic events as observed at LEP. The events were passed through a full simulation of the OPAL detector [13] as well as the event reconstruction software and finally subjected to the same selection process as for the real data.

In addition to this JETSET Monte Carlo sample, 140 000 fully simulated events were taken from a Monte Carlo program based on the default HERWIG 5.5 model [14]. This sample was used to check for systematic effects which may arise from the JETSET model of fragmentation. The HERWIG events were also used to determine the experimental acceptance for the $\mathrm{K}_2^*(1430)^0$ analysis since the JETSET event sample did not contain tensor mesons.

To correct for shortcomings in the simulation of track matching between the jet chamber and z-chambers in the central tracking system, a weight was assigned to each of the selected Monte Carlo tracks. These weights were based on a study in both data and Monte Carlo of the distribution of transverse momentum and polar angle of tracks which included z information from the z-chambers. These weights varied between 0.94 and 1.08, with a mean value of 1.01. The overall uncertainty in these weights, which amounted to 0.8%, was taken into account in the final evaluation of systematic uncertainties.

3 Particle identification

Particle identification was carried out on a track by track basis using ionisation energy loss ($\mathrm{d}E/\mathrm{d}x$) information. Each track was required to have at least 20 separate points of $\mathrm{d}E/\mathrm{d}x$ measurement in the central tracking chamber and ionisation loss less than 40 keV/cm, in order to remove tracks that would not be well simulated. Given that the separation in mean $\mathrm{d}E/\mathrm{d}x$ between particle types depends strongly on momentum [15] it was not possible to identify kaons across the entire momentum range. A study of this effect was carried out in [4] and the same limits were applied in the present analysis: no tracks were identified as kaons between 0.8 and 2.0 GeV/c.

For a given track a χ^2 probability, or $\mathrm{d}E/\mathrm{d}x$ weight, was calculated for each of the four candidate particle types (electrons, pions, kaons and protons). If at least one of the four weights was above 0.05 then the track was assigned to the particle type corresponding to the largest χ^2 probability. Using this procedure on the data, 10.23 tracks per event on average were assigned a particle type. The difference in mean track multiplicity between real data and the weighted Monte Carlo sample was only 0.6% for all tracks and 0.3% for those tracks with a particle type assigned to them from the identification process.

4 Two-particle invariant mass spectra

For each event the KK two-particle invariant mass was calculated for all two track combinations where both tracks were identified as kaons. The Kπ invariant mass was constructed for each kaon candidate combined with all the other tracks in the event. Pion identification was not used in the construction of the Kπ mass spectra as it would introduce further systematic uncertainty to the measurement without a significant reduction in the background. The invariant mass spectra were formed in various ranges of the scaled energy variable x_E defined by

$$x_E = E/E_{\rm beam} \ , \tag{1}$$

where E is the combined energy of the two particles and $E_{\rm beam}$ is the LEP beam energy for the event. In the analysis of the KK spectra six regions of x_E were considered, while the data were split into 10 regions for the Kπ plots.

Separate histograms were used to record neutral and doubly charged combinations. Figures 1 and 2 show the resultant mass spectra for KK and Kπ combinations, integrated over x_E. The JETSET Monte Carlo plots have been normalised to the same total number of selected Z^0 decay events as the data, in order to make a direct comparison.

In the KK spectra the $\phi(1020)$ signal is clearly visible in the neutral combinations. Apart from the intensity of the signal, the Monte Carlo simulates the shape of the data well, although there are small discrepancies in both plots just above threshold. This may be due partly to the effects of Bose-Einstein correlations which are not simulated in the Monte Carlo.

In the Kπ mass spectra the signal to background ratio for the $K^*(892)^0$ is much smaller than for the $\phi(1020)$ due mainly to the large excess of combinatorial Kπ pairs in comparison to KK combinations. In order to enhance the signal, the spectra for doubly charged Kπ combinations were subtracted from those for neutral combinations on a bin by bin basis; the resultant 'subtracted' plot is shown for the entire x_E range in figure 3.

As the simulated events contain a record of the origin of each measured track it is possible to break down the JETSET Monte Carlo invariant mass spectra into their constituent parts. Some of the main features of the KK and Kπ mass spectra are shown in figures 4 and 5. These consist of the signal, the combinatorial background and backgrounds from the decay of other states, where one or both of the decay particles have been misidentified, resulting in a distorted signal from the miscalculated invariant mass (referred to as reflections). One particularly important background of this type is from the decay of the $\rho(770)^0$ to two charged pions. According to the Monte Carlo the reflection lies under the $K^*(892)^0$ peak so that a good understanding of this background is vital to the analysis.

5 Particle identification efficiency

As the Monte Carlo sample is used extensively in the analysis it is important to check the consistency of particle identification efficiencies between the simulated data and those measured from the detector. To this end, efficiencies for kaon identification were measured directly from the invariant mass spectra in the real data and compared to values deduced from the Monte Carlo simulation.

For each of the K^+K^- mass plots in the real data (in 6 bins of x_E) the $\phi(1020)$ signal was fitted using the appropriate Monte Carlo background and a signal shape parametrised using

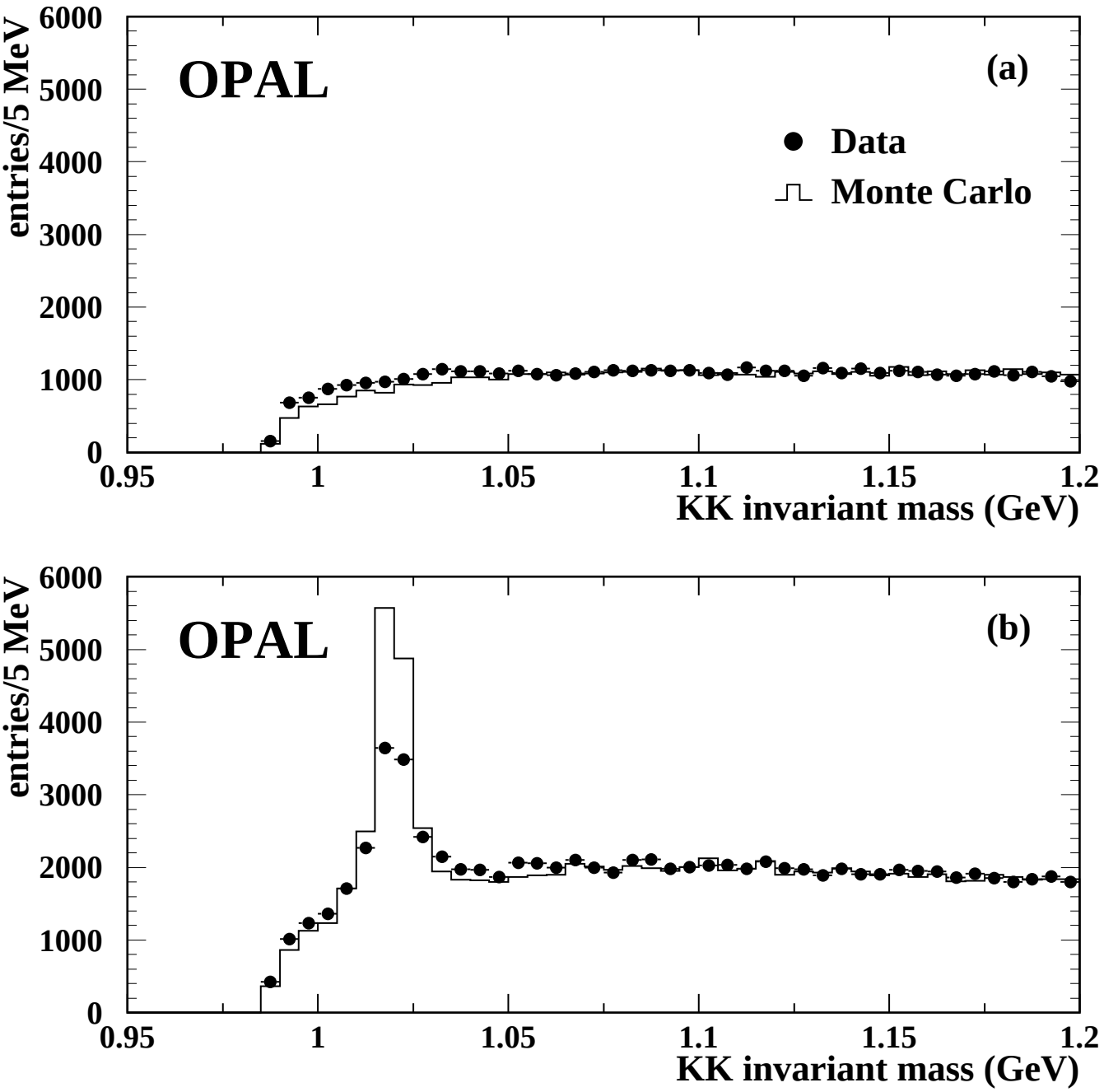

Figure 1: Two-particle invariant mass spectra for (a) selected $K^{\pm}K^{\pm}$ combinations, (b) selected $K^{\pm}K^{\mp}$ combinations.

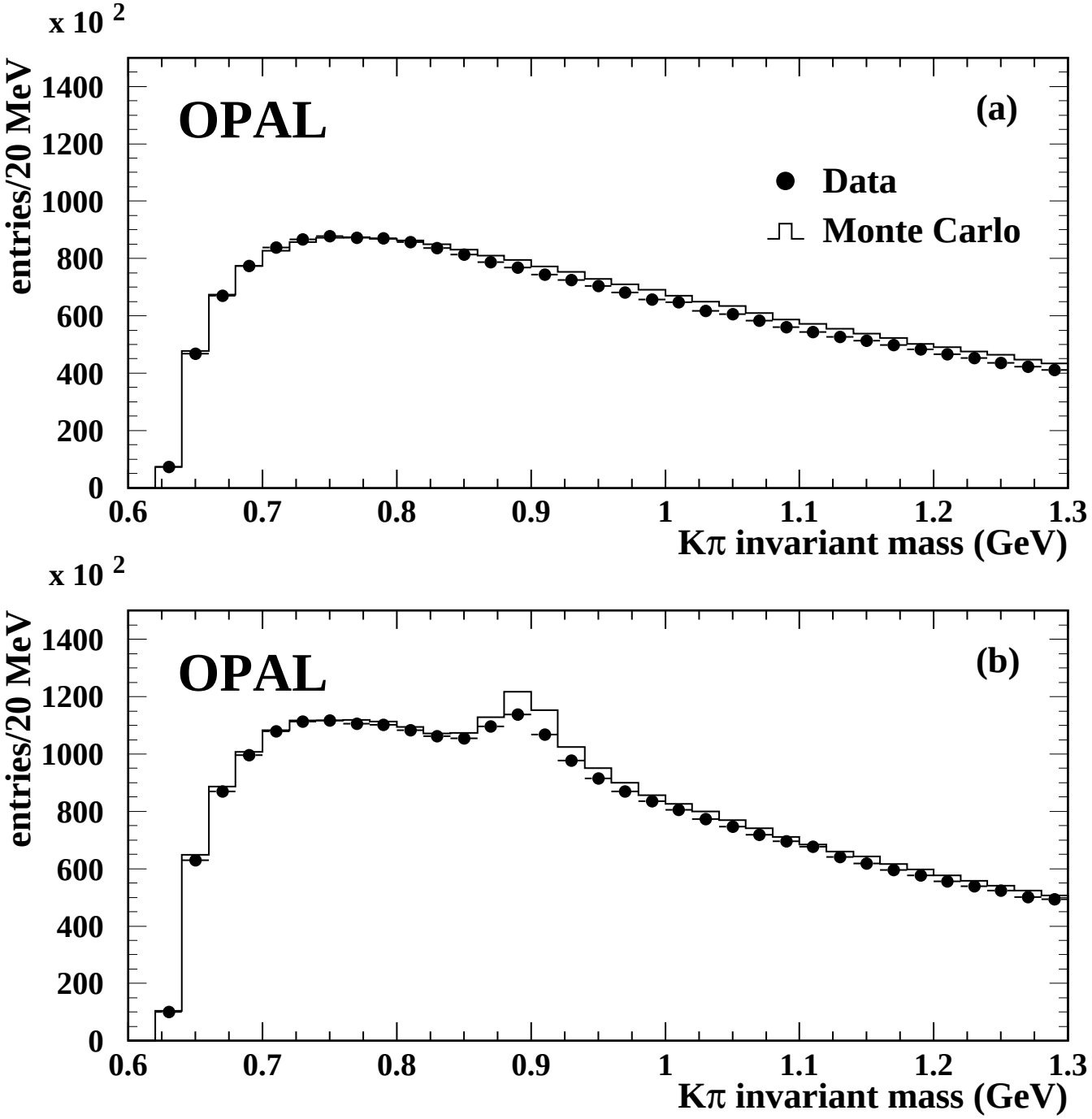

Figure 2: Two-particle invariant mass spectra for (a) selected $K^{\pm}\pi^{\pm}$ combinations, (b) selected $K^{\pm}\pi^{\mp}$ combinations.

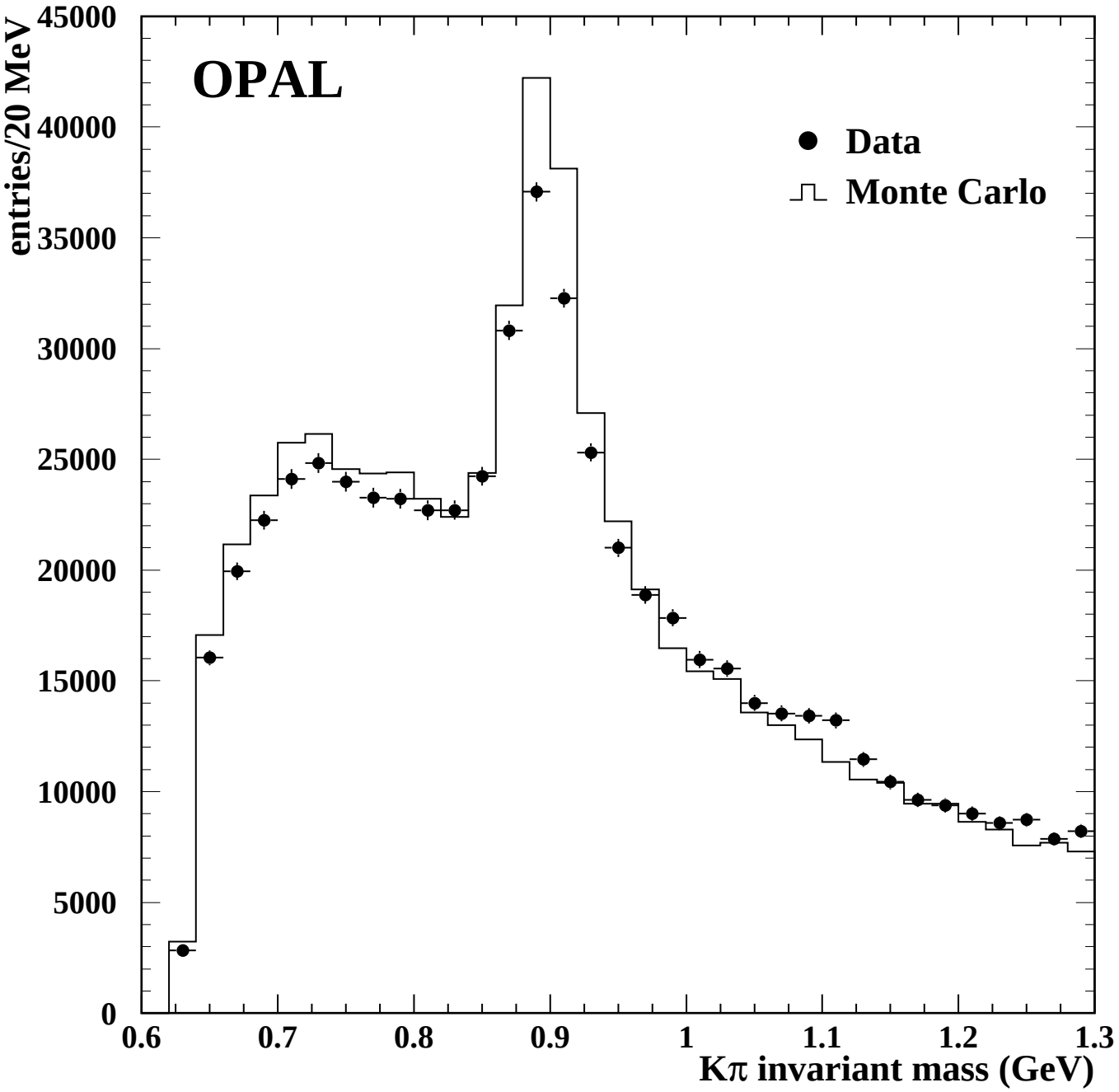

Figure 3: Two-particle 'subtracted' invariant mass spectra for selected Kπ combinations.

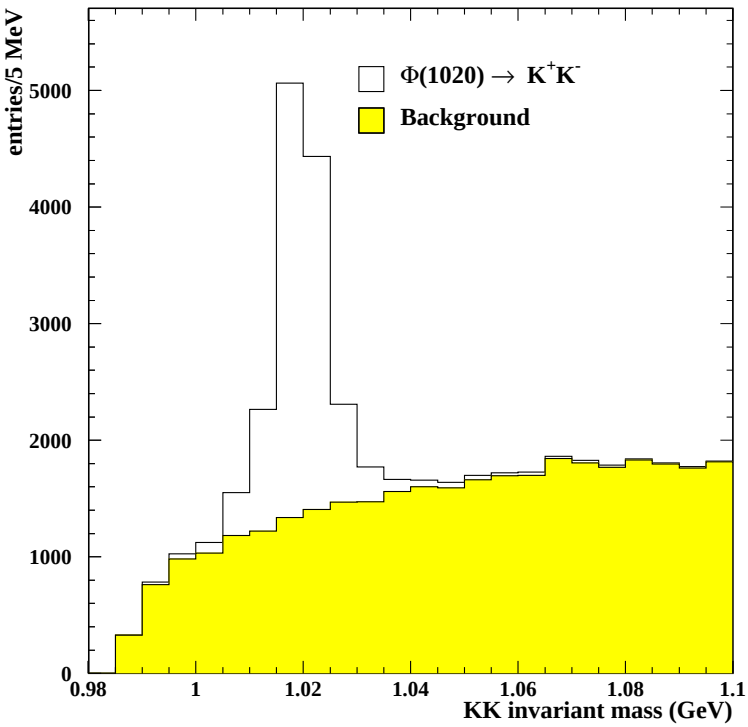

Figure 4: Composition of the JETSET Monte Carlo K^+K^- mass spectrum.

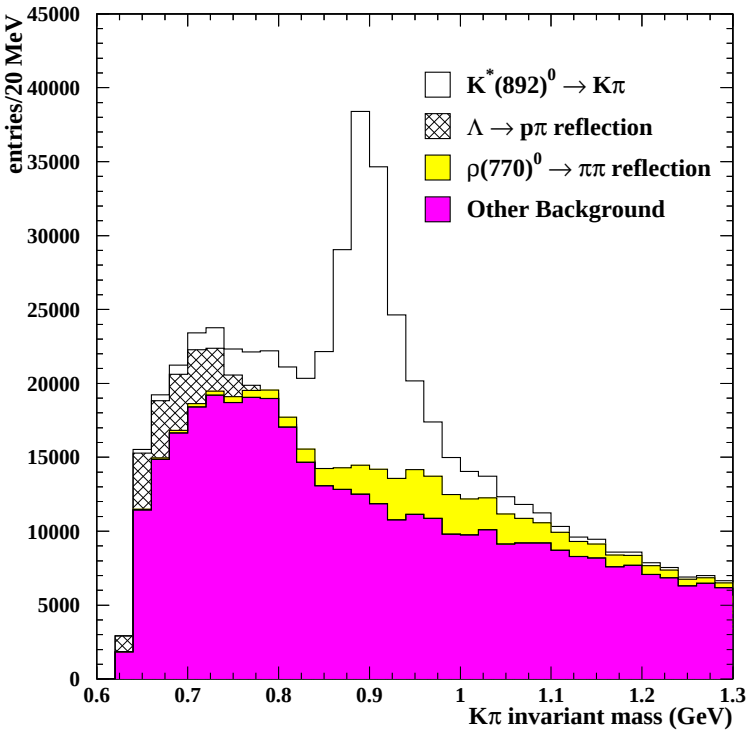

Figure 5: Composition of the 'subtracted' JETSET Monte Carlo $K\pi$ mass spectrum.

x_E region for ϕ	$\eta_{\rm data}$	$\eta_{\rm MC}$	$\eta_{\rm MC}/\eta_{\rm data}$
0.025 – 0.071	0.78 ± 0.05	0.799 ± 0.010	1.02 ± 0.07
0.071 – 0.150	0.87 ± 0.04	0.830 ± 0.005	0.96 ± 0.05
0.150 – 0.215	0.85 ± 0.05	0.837 ± 0.006	0.99 ± 0.06
0.215 – 0.300	0.78 ± 0.05	0.824 ± 0.006	1.06 ± 0.07
0.300 – 0.454	0.78 ± 0.05	0.818 ± 0.007	1.04 ± 0.07
0.454 – 1.000	0.80 ± 0.07	0.777 ± 0.010	0.97 ± 0.08

Table 1: Comparison of kaon identification efficiencies for data and Monte Carlo.

the convolution of a relativistic Breit-Wigner and a Gaussian to account for the experimental resolution. The particle identification criteria were then relaxed so that in each two track combination only one track was required to be identified as a kaon. The fits were repeated on the resultant mass spectra using the same signal parametrisation. From these fits the kaon identification efficiency, $\eta_{\rm K}$, can be evaluated using

$$\eta_{\rm K} = \frac{2I_{\rm KK}/I_{\rm Kx}}{1 + I_{\rm KK}/I_{\rm Kx}} \ , \tag{2}$$

where $I_{\rm KK}$ and $I_{\rm Kx}$ are the ϕ meson intensities measured from the two sets of mass plots. This procedure was repeated on the JETSET Monte Carlo mass spectra. The kaon identification efficiency in $\phi(1020)$ decays was also measured directly from the Monte Carlo sample using the knowledge of the generated and reconstructed type of each track. The two sets of Monte Carlo efficiencies were found to agree, and so the latter values, with smaller errors, were used to compare with the data. The results of this study are given in table 1. In all the x_E regions the data and Monte Carlo kaon identification efficiencies agree. The factors $(\eta_{\rm MC}/\eta_{\rm data})^2$ were applied as corrections to the measured $\phi(1020)$ production rates and the uncertainties on these ratios were included as part of the overall systematic error, taken to be uncorrelated from bin to bin in x_E. As the kaons resulting from the $\phi(1020)$ decays used in this study cover a large momentum band it was assumed that the data and Monte Carlo identification efficiencies are comparable for all kaons, including for example those from $\rm K^*(892)^0$ decays. The average value of $\eta_{\rm MC}/\eta_{\rm data}$ in table 1, which amounted to 1.0, was used in the determination of the $\rm K^*(892)^0$ multiplicity and the average of the errors on these ratios, ± 0.07, was assigned as part of the systematic uncertainty, again taken to be uncorrelated from bin to bin.

To check the assumptions made in estimating the uncertainty for each individual x_E bin an alternative treatment was also considered. The mass spectra summed over all six x_E bins were fitted as described above, both for data and Monte Carlo, and the overall kaon identification efficiency extracted. The ratio $\eta_{\rm MC}/\eta_{\rm data}$ was found to be 1.00 ± 0.03. The error on this ratio was used to calculate the contribution to the systematic uncertainty on the total measured $\phi(1020)$ and $\rm K^*(892)^0$ rates. The difference in the systematic errors determined from this treatment and the one described above was found to be negligible.

x_E Region	x_{lw}	Multiplicity /Z^0 decay	$1/\sigma_{\rm had}\,(d\sigma/dx_E)$
0.025 – 0.071	0.046	$0.031 \pm 0.003 \pm 0.005$	$0.67 \pm 0.07 \pm 0.12$
0.071 – 0.150	0.108	$0.028 \pm 0.002 \pm 0.003$	$0.35 \pm 0.02 \pm 0.04$
0.150 – 0.215	0.182	$0.013 \pm 0.001 \pm 0.002$	$0.20 \pm 0.01 \pm 0.03$
0.215 – 0.300	0.256	$0.011 \pm 0.001 \pm 0.002$	$0.13 \pm 0.01 \pm 0.02$
0.300 – 0.454	0.372	$0.010 \pm 0.001 \pm 0.002$	$0.06 \pm 0.005 \pm 0.01$
0.454 – 1.000	0.654	$0.005 \pm 0.001 \pm 0.001$	$0.01 \pm 0.001 \pm 0.002$
0.023 – 0.025	-	0.002^*	-
0.023 – 1.000	-	$0.100 \pm 0.004 \pm 0.007$	-

* - Unobserved region, multiplicity determined using JETSET 7.3 and HERWIG 5.5

Table 2: Results for inclusive $\phi(1020)$ production.

6 Inclusive $\phi(1020)$ and $K^*(892)^0$ production

6.1 Fitting the K^+K^- mass spectra

The K^+K^- mass spectra were fitted using the minimum χ^2 method in exactly the same manner as in the earlier analysis [4]. The plots representing the six x_E regions were fitted over an invariant mass range from the KK threshold up to 1.06 GeV. In each x_E region the shapes of the signal and background contributions were extracted from the appropriate Monte Carlo mass spectra. In the fit the signal intensity and the level of combinatorial background were allowed to vary; all other contributions to the Monte Carlo mass spectra were small and were fixed at their default values. Systematic effects which may arise due to discrepancies between the $\phi(1020)$ signal shape in the data and the simulation are discussed in section 6.4.

The results of the fits for each of the x_E bins are shown in figure 6. As the Monte Carlo mass spectra used for the fits had been normalised to the same number of Z^0 decays as in the data, the results were a direct measurement of the data to Monte Carlo intensity ratio for the $\phi(1020)$. The production rate in each of the x_E regions could then be determined by scaling the JETSET multiplicities and taking into account the corrections for particle identification efficiency calculated as described in section 5. To account for the small unobserved region at low x_E the Monte Carlo behaviour was assumed. Both JETSET 7.3 and HERWIG 5.5 were found to predict the same correction. The measured rates for each of the x_E bins are given in table 2 and the overall multiplicity was determined to be $0.100 \pm 0.004 \pm 0.007$ per event. The first quoted error is statistical and the second is an estimate of the systematic error on the measurement, taken to be uncorrelated from bin to bin in x_E. The scaled energy value, x_{lw}, referred to in the table, is the appropriate position within the x_E bin used to plot the differential cross section, as discussed in section 6.3.

6.2 Fitting the $K\pi$ mass spectra

As was pointed out earlier, an understanding of the $\rho(770)^0$ reflection in the $K\pi$ mass spectra is essential in the determination of the $K^*(892)^0$ production rate. A study of the $\pi^+\pi^-$ invariant mass spectra in [4], and more recently in [16], revealed a marked difference between the data

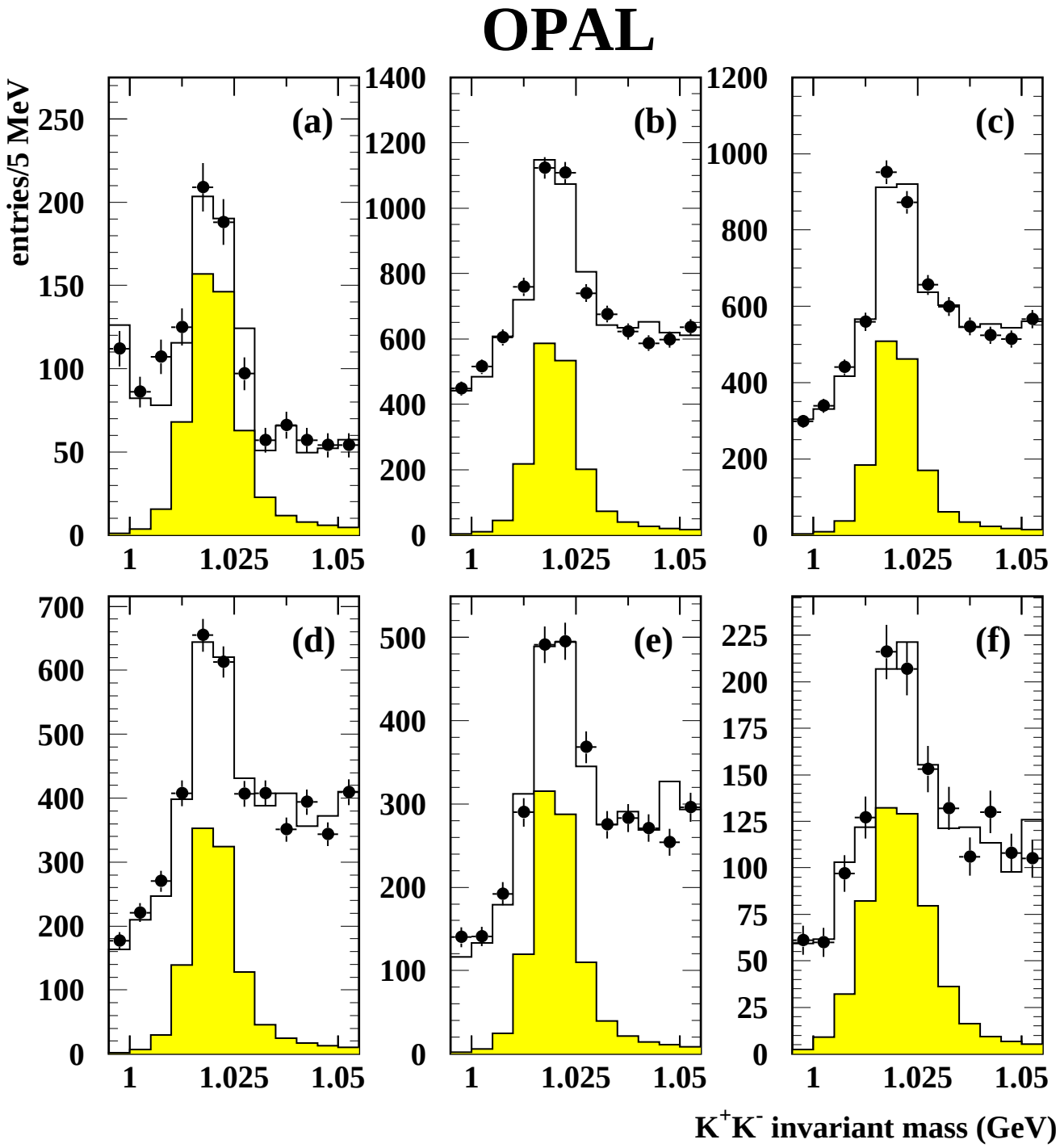

Figure 6: Fits to the K^+K^- invariant mass plots in six bins of x_E: (a) $0.025 < x_E < 0.071$, (b) $0.071 < x_E < 0.150$, (c) $0.150 < x_E < 0.215$, (d) $0.215 < x_E < 0.300$, (e) $0.300 < x_E < 0.454$, (f) $0.454 < x_E < 1.000$. The open histograms show the results of the fits, and the shaded plots are the extracted $\phi(1020)$ signals.

and JETSET Monte Carlo signal shapes for $\rho(770)^0$. It was suggested that the distortion could be due to Bose-Einstein correlations which were not simulated in the default version of JETSET. A further study of the effect on the $\rho(770)^0$ line shape of these correlations and other mechanisms was reported in [17]. There it was suggested that the shape of the ρ^0 signal in $\pi^+\pi^-$ mass spectra could be parametrised as a distorted relativistic Breit-Wigner, written for a mass m as

$$I(m) = R(m)\left[1 + C\left(\frac{m_\rho^2 - m^2}{m\Gamma}\right)\right] \ , \tag{3}$$

where Γ is the mass dependent width of the relativistic Breit-Wigner $R(m)$ [18] and C is a variable parameter which depends on the momentum of the ρ^0, varying from around 1.0 at low values of scaled momentum x_p, down to zero for high momenta. The overall effect of equation (3) is to move the peak of the ρ^0 background to a lower mass, by up to 40 MeV for C equal to one.

In order to study the effect of this on the ρ^0 background in the Kπ mass spectra, reflections were generated using the following procedure. Two body $\rho^0 \rightarrow \pi^+\pi^-$ decays were generated using the Monte Carlo program GENBOD [19] with a line shape determined from the parametrisation given above. The behaviour of C was represented simply by $(1 - x_p)$ with the momentum spectrum of the ρ^0 mesons taken from JETSET.

Using the track origin information in the JETSET Monte Carlo event sample, histograms were constructed of the variation of $\pi \rightarrow$K misidentification probability with momentum. These probabilities were used to create Kπ reflections from the generated $\rho^0 \rightarrow \pi^+\pi^-$ decays. The reflections were plotted in the same bins of x_E as used in the $K^*(892)^0$ analysis. Using the same procedure a second set of reflections was generated using a normal Breit-Wigner function as input to GENBOD rather than the above parametrisation.

Three separate sets of fits were made to the Kπ mass spectra over an invariant mass range from 0.64 to 1.2 GeV. For the first fits, the JETSET $\rho(770)^0$ shape (a simple non-relativistic Breit-Wigner) was used, but for the other two the reflections generated using GENBOD, with and without distortions, were included instead, with the intensity normalised to the JETSET value in each case. For all the fits the $K^*(892)^0$ signal shape was taken from the Monte Carlo mass spectra, the intensity from the $\phi(1020)$ background was fixed to values obtained from earlier fits to the KK spectra and all other non combinatorial backgrounds were set at JETSET levels. The fitted spectra using the JETSET $\rho(770)^0$ reflections are shown in figure 7.

The fit results using the JETSET ρ^0 reflection and those with generated ρ^0 shapes with no distortions were consistent. This indicated that the generated reflections from GENBOD were reliable even though they had not been passed through a full detector simulation. When the ρ^0 reflections included distortion effects as parametrised by equation (3) the fitted $K^*(892)^0$ intensity was consistently lower. This was to be expected as the distortion effects move the reflected ρ^0 peak down in mass closer to the $K^*(892)^0$, thus reducing the effective fitted K^* intensity.

The mean of the two fit values for each x_E bin obtained using the parametrised ρ^0 reflections (with and without distortions) was used to calculate the overall $K^*(892)^0$ production rate. Half of the difference between the two was used as an estimate of the systematic uncertainty due to the $\rho(770)^0$ reflection. As in the $\phi(1020)$ analysis a small correction was applied for the unobserved region in x_E based on JETSET and HERWIG predictions. The measured rates for each of the x_E regions are given in table 3. The overall production rate was determined to be $0.74 \pm 0.03 \pm 0.03$ $K^*(892)^0$ mesons per hadronic Z^0 decay.

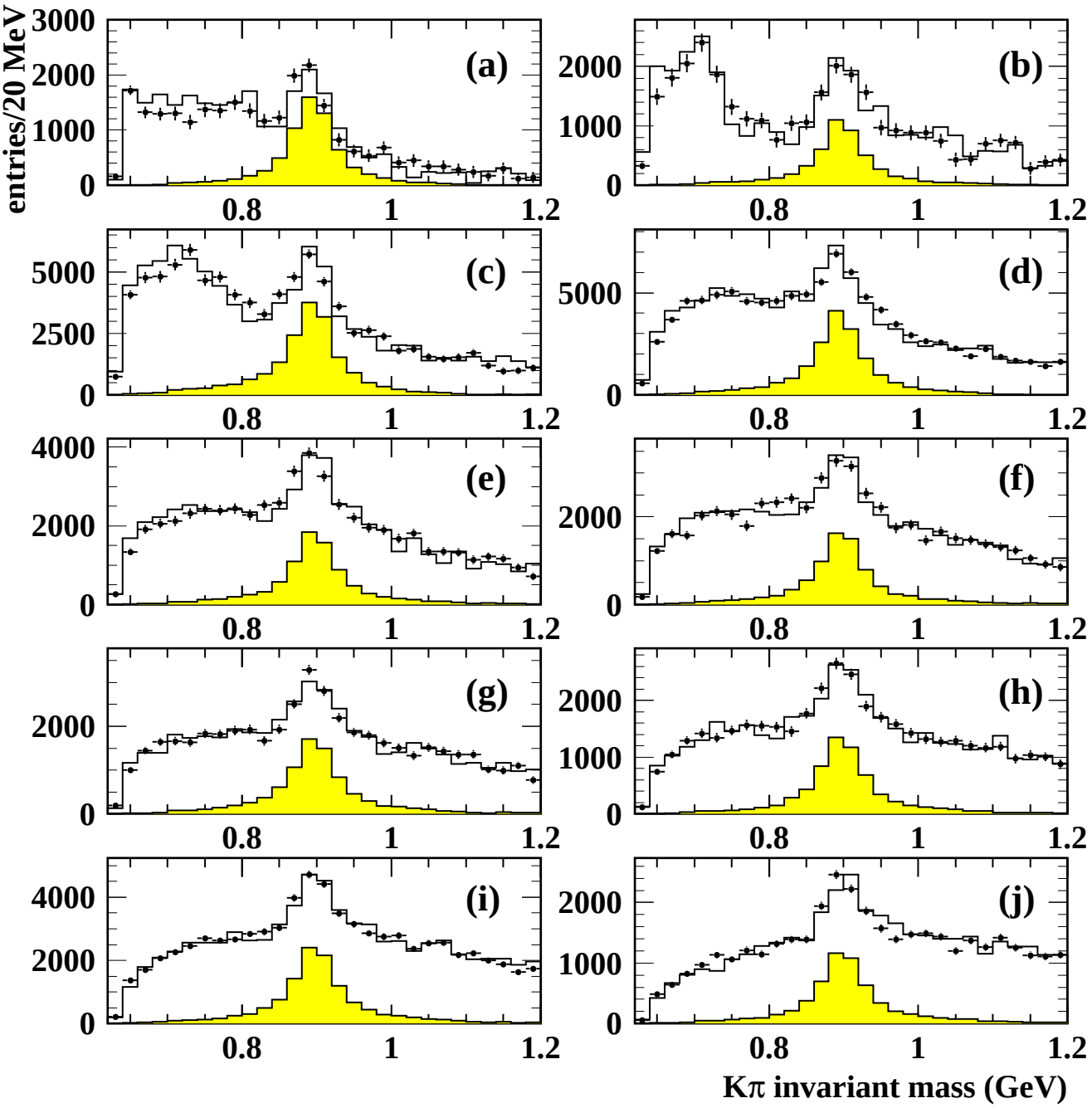

Figure 7: Fits to the Kπ invariant mass plots in ten bins of x_E: (a) $0.021 < x_E < 0.044$, (b) $0.044 < x_E < 0.071$, (c) $0.071 < x_E < 0.107$, (d) $0.107 < x_E < 0.150$, (e) $0.150 < x_E < 0.180$, (f) $0.180 < x_E < 0.215$, (g) $0.215 < x_E < 0.255$, (h) $0.255 < x_E < 0.300$, (i) $0.300 < x_E < 0.454$, (j) $0.454 < x_E < 1.000$. The open histograms show the results of the fits, and the shaded plots are the extracted $K^*(892)^0$ signals.

x_E Region	x_{lw}	Multiplicity /Z^0 decay	$1/\sigma_{\rm had}\,(d\sigma/dx_E)$
0.021 – 0.044	0.033	$0.151 \pm 0.014 \pm 0.010$	$6.56 \pm 0.61 \pm 0.43$
0.044 – 0.071	0.057	$0.121 \pm 0.019 \pm 0.016$	$4.48 \pm 0.70 \pm 0.59$
0.071 – 0.107	0.088	$0.133 \pm 0.008 \pm 0.015$	$3.69 \pm 0.22 \pm 0.42$
0.107 – 0.150	0.127	$0.097 \pm 0.006 \pm 0.009$	$2.25 \pm 0.14 \pm 0.21$
0.150 – 0.180	0.165	$0.040 \pm 0.004 \pm 0.004$	$1.33 \pm 0.13 \pm 0.13$
0.180 – 0.215	0.197	$0.037 \pm 0.004 \pm 0.004$	$1.06 \pm 0.11 \pm 0.11$
0.215 – 0.255	0.234	$0.041 \pm 0.003 \pm 0.004$	$1.02 \pm 0.08 \pm 0.10$
0.255 – 0.300	0.278	$0.031 \pm 0.003 \pm 0.003$	$0.69 \pm 0.07 \pm 0.07$
0.300 – 0.454	0.372	$0.055 \pm 0.003 \pm 0.005$	$0.36 \pm 0.02 \pm 0.03$
0.454 – 1.000	0.661	$0.026 \pm 0.002 \pm 0.002$	$0.05 \pm 0.004 \pm 0.004$
0.020 – 0.021	-	0.011^*	-
0.020 – 1.000	-	$0.743 \pm 0.027 \pm 0.027$	-

* - Unobserved region, multiplicity determined using JETSET 7.3 and HERWIG 5.5

Table 3: Results for inclusive $K^*(892)^0$ production.

6.3 Differential cross sections

For both the $\phi(1020)$ and $K^*(892)^0$ mesons, normalised differential cross sections were calculated and plotted as a function of x_E. To determine the appropriate positions for the data points within the x_E bins, the procedure recommended in [20] was used. Both HERWIG and JETSET curves in each bin were considered, but significant differences in the calculated positions were found only for the highest x_E region, which corresponded to the widest bin. For this point the mean of the two positions was used and the difference was taken to be the uncertainty on the x_E position in the bin. The resulting values, x_{lw}, are given in tables 2 and 3. The results are shown in figures 8 and 9 together with the fragmentation functions for JETSET 7.3 and HERWIG 5.5. The x_E bin limits are also shown on the plots, in the manner recommended in [20]. The fragmentation function is also shown for JETSET with two parameters tuned as described in [4] to reproduce a number of measured production rates. The JETSET parameters altered were: the strangeness suppression factor, PARJ(2), was set to 0.245 (the default value is 0.3) and the probability that a strange meson will have spin 1, PARJ(12), was changed from 0.6 to 0.43.

For a comparison with measurements of other hadron states the entire $\phi(1020)$ and $K^*(892)^0$ analyses were repeated using bins of the variable $\xi = \ln(1/x_p)$, where x_p is the scaled meson momentum, rather than x_E. The modified leading log approximation in QCD with local parton-hadron duality (MLLA+LPHD) [21] predicts that differential cross sections with respect to this variable should have a Gaussian-like shape. Figures 10 and 11 show the measured distributions for $\phi(1020)$ and $K^*(892)^0$ along with the Gaussian fits used to measure the peak positions. The values of $\xi_{\rm peak}$ were determined to be 2.29 ± 0.05 and 2.40 ± 0.04 for the $\phi(1020)$ and $K^*(892)^0$ respectively.

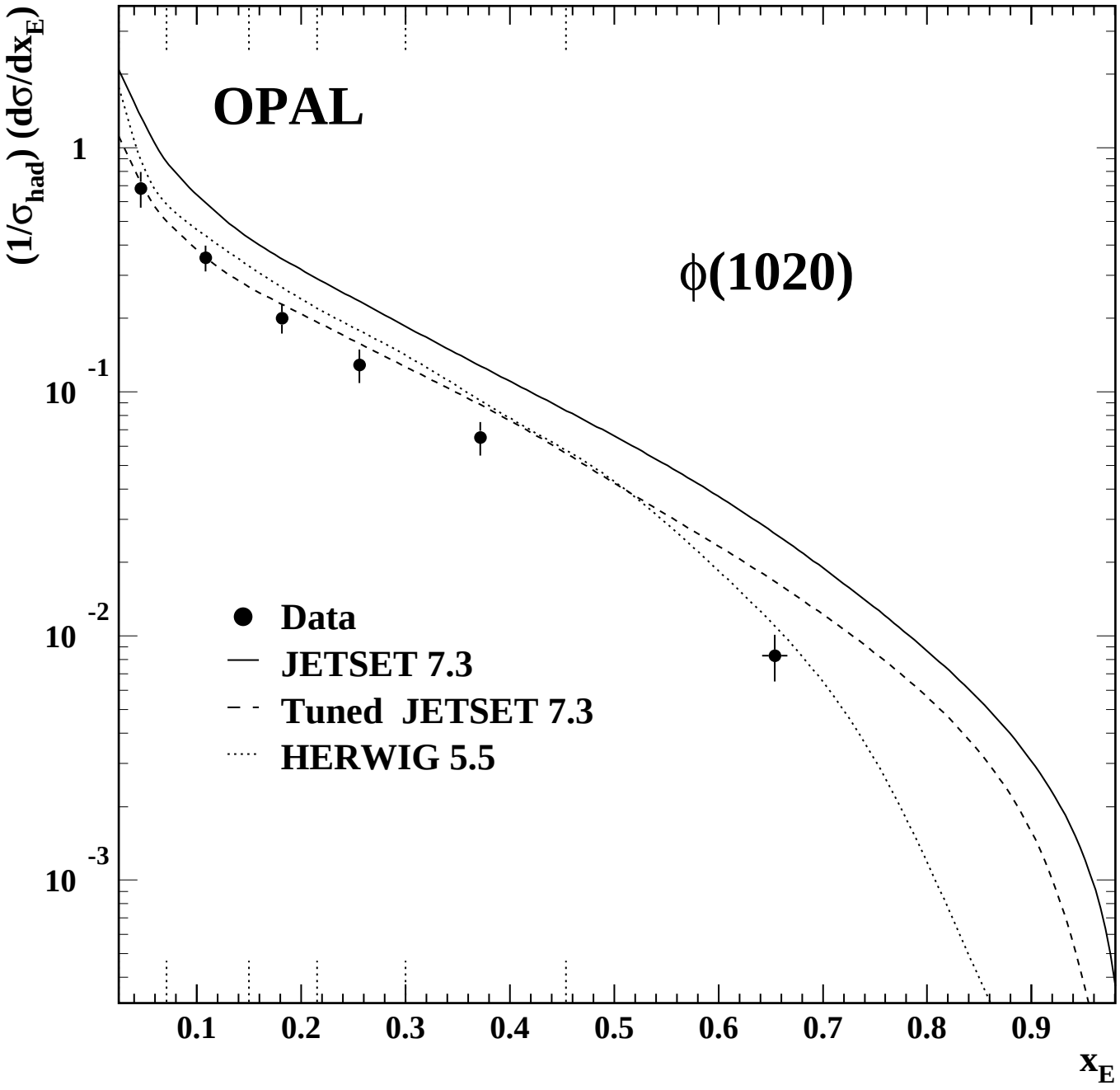

Figure 8: Differential cross sections for measured and simulated $\phi(1020)$ production. The solid curve indicates the prediction of JETSET 7.3 using default parameters and the dashed curve shows the result of tuning JETSET as described in section 6.3. The HERWIG 5.5 prediction is displayed as a dotted curve. The error bars show the combined statistical and systematic uncertainty on each point. The bin ranges are indicated by means of the short vertical lines at the top and bottom of the plot.

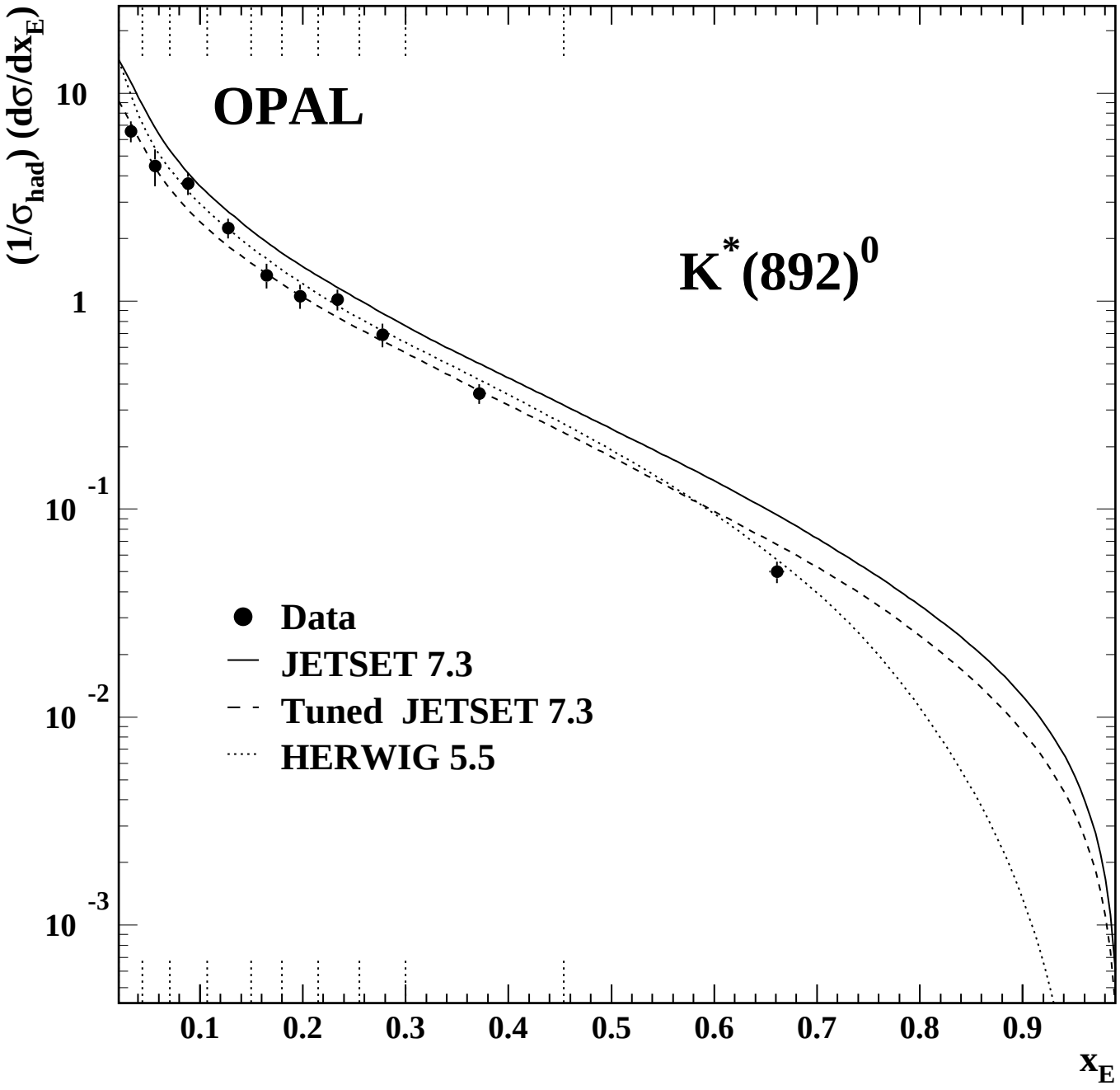

Figure 9: Differential cross sections for measured and simulated $K^*(892)^0$ production. The solid curve indicates the prediction of JETSET 7.3 using default parameters and the dashed curve shows the result of tuning JETSET as described in section 6.3. The HERWIG 5.5 prediction is displayed as a dotted curve. The error bars show the combined statistical and systematic uncertainty on each point. The bin ranges are indicated by means of the short vertical lines at the top and bottom of the plot.

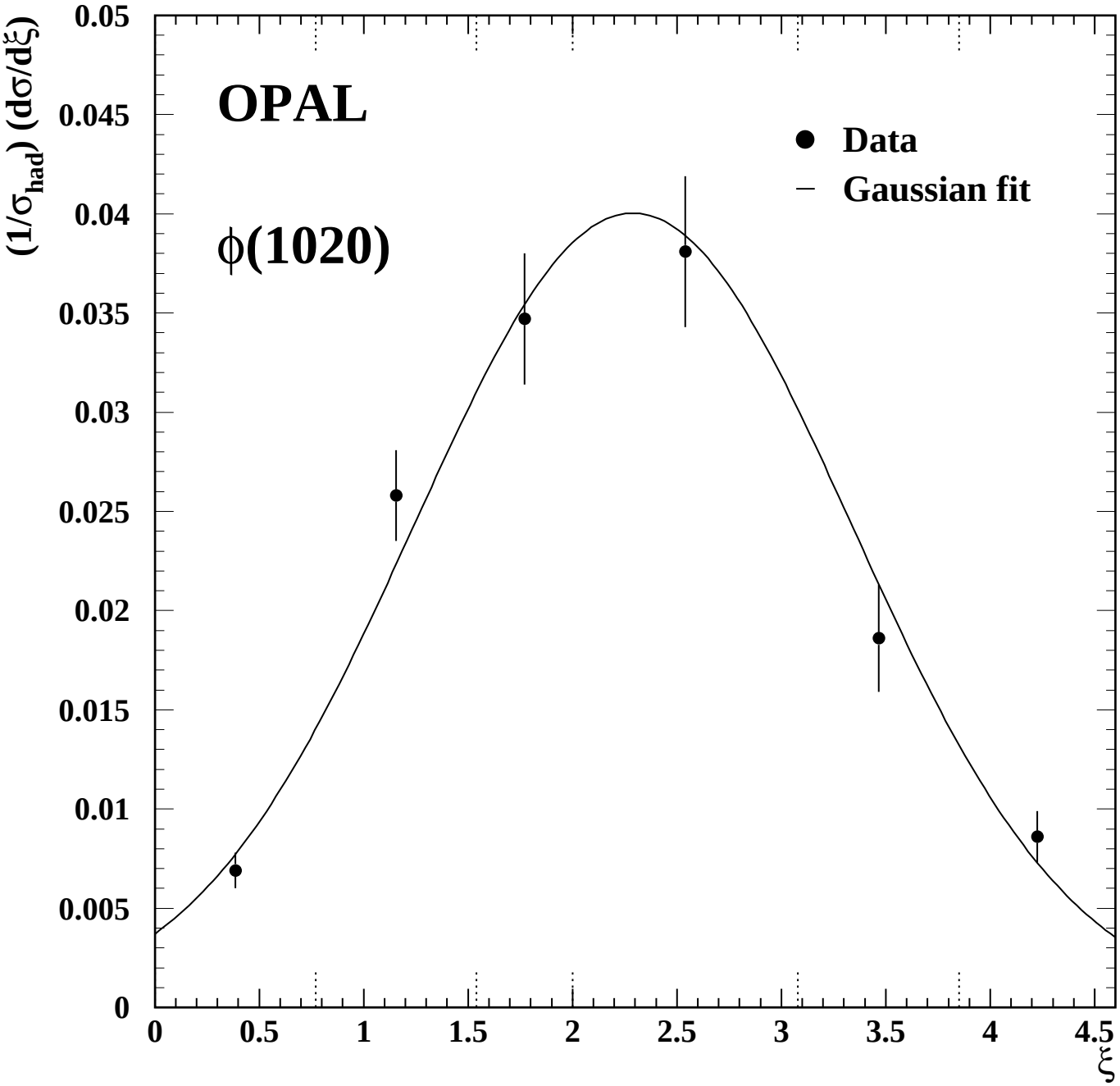

Figure 10: Differential cross section for $\phi(1020)$ as a function of $\xi = \ln(1/x_p)$. The error bars show the combined statistical and systematic uncertainty on each point. The bin ranges are indicated by means of the short vertical lines at the top and bottom of the plot.

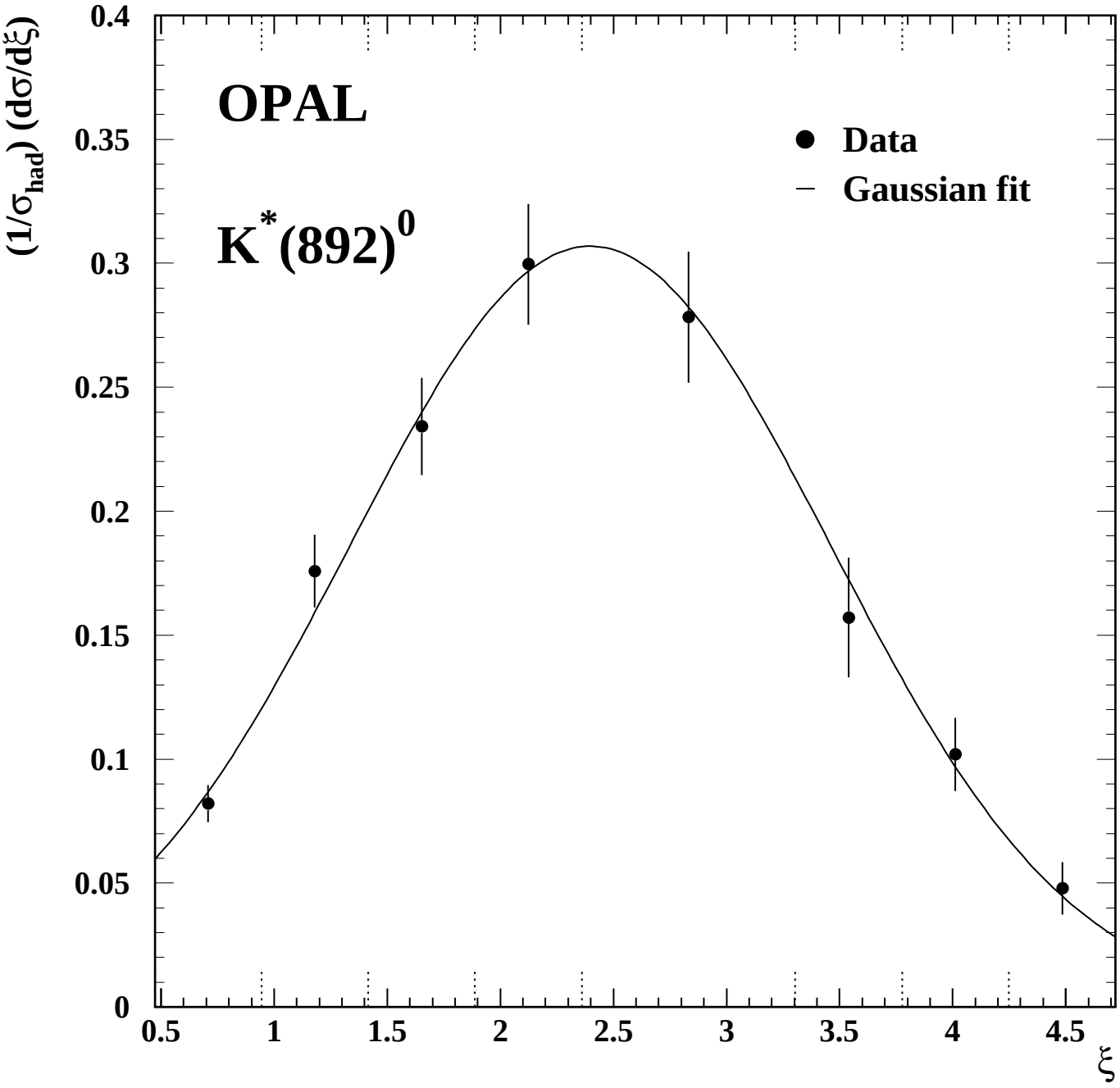

Figure 11: Differential cross section for $K^*(892)^0$ as a function of $\xi = \ln(1/x_p)$. The error bars show the combined statistical and systematic uncertainty on each point. The bin ranges are indicated by means of the short vertical lines at the top and bottom of the plot.

6.4 Systematic errors

The effects on the production rates of the $\phi(1020)$ and $K^*(892)^0$ from the various sources of systematic error investigated are summarised in table 4.

The normalisation procedure used to compare the data and Monte Carlo samples resulted in an overall 1.4% error on the final multiplicities. This came from both the reweighting of Monte Carlo events to account for matching inefficiencies between the central jet chamber and outer z-chambers and from the model dependence of the quality cuts.

The systematic effects due to uncertainties in the kaon particle identification were calculated using the errors on the efficiency measurements described in section 5 above. The outcome of this was a 5.6% uncertainty on the $\phi(1020)$ multiplicity and a 2.4% error on the $K^*(892)^0$. These values turned out to be the largest contributions to the systematic errors. However it must be noted that they stem from the fits used in the efficiency measurements and should decrease in magnitude with increased statistics.

As the $\phi(1020)$ is a narrow state with a natural width similar to the intrinsic mass resolution of the detector, discrepancies in the shape of the state between the data and Monte Carlo may have a systematic effect on the fits. To test this, both the data and JETSET Monte Carlo K^+K^- mass spectra were fitted to a combination of a relativistic Breit-Wigner convolved with a Gaussian (the same signal shape as used in the efficiency calculations), and a Weibull function [22] to represent the background. The width of the Gaussian part, which provides a measure of the resolution of the signal, was found to be compatible between the two data sets. The fits were then repeated for the data mass spectra with the resolution fixed at ± 1 standard deviation from the fitted resolution in the Monte Carlo. Using this procedure the intensity of the $\phi(1020)$ signal was found to vary by 1%. For the $K^*(892)^0$ meson, which has a width much greater than the two-particle mass resolution of the detector, such systematic effects were found to be negligible.

Bose-Einstein correlations and residual correlations represent a source of systematic errors in the two vector states. For the $\phi(1020)$ the systematic errors for this effect were taken directly from the published work [4] where a reweighting technique was used to simulate the effect in the Monte Carlo mass plots. A 3.5% effect on the overall rate is reported from the study and this was included in the systematics in the present analysis. For the $K^*(892)^0$ the effect is indirect, occurring in $\pi^+\pi^-$ systems which are reflected into the $K\pi$ mass plots due to $\pi \rightarrow K$ misidentification. This effect has been studied as reported in section 6.2.

As there is some difficulty in measuring reliably the $\rho(770)^0$ production rate in Z^0 decay [4, 6, 7, 16, 17], mainly due to problems in understanding the line shape, the effect of varying the intensity of the reflection in the mass plots was studied. It was found that a variation of $\pm 30\%$ in the ρ^0 intensity resulted in only a 1.2% change in the fitted $K^*(892)^0$ intensity and had a negligible effect on the $\phi(1020)$. Finally a 1.8% uncertainty was added to the systematic error on the measured $\phi(1020)$ rate to account for the uncertainty on the $\phi \rightarrow K^+K^-$ branching ratio [23].

7 Inclusive $K_2^*(1430)^0$ production

As the $K_2^*(1430)^0$ is a wide state, with a natural width of 109 MeV [23], additional cuts were introduced to obtain an improved signal to background ratio in the $K\pi$ mass spectra. In order

Source of systematic error	Error on $\phi(1020)$ rate	Error on $K^*(892)^0$ rate
Normalisation of Monte Carlo	± 0.0014	± 0.010
Particle identification efficiency	± 0.0056	± 0.018
Mass resolution	± 0.0010	-
Bose-Einstein effects	± 0.0035	± 0.015
$\rho(770)^0$ intensity	-	± 0.009
Branching ratio	± 0.0018	-
Total	± 0.0071	± 0.027

Table 4: Systematic uncertainties on $\phi(1020)$ and $K^*(892)^0$ rates.

to reduce the combinatorial background from $K\pi$ and $\pi\pi$ pairs the selected tracks were required to pass more stringent quality cuts before particle identification was attempted. The minimum number of points of dE/dx measurement was increased from 20 to 100 and tracks were required to have at least five z space point measurements in the z-chambers. It was found that improving the dE/dx and momentum measurement in this way was more effective than tightening the cuts made on the dE/dx weights. The kaon identification efficiencies for both data and Monte Carlo were re-evaluated for this new set of cuts, following the procedures described in section 5.

The $K\pi$ two-particle invariant mass spectra were plotted by combining identified kaons with all the other tracks in each event. Two regions of x_E were considered, up to 0.3 and from 0.3 to 1.0. As in the $K^*(892)^0$ analysis the histograms for like and unlike charge combinations were subtracted bin by bin to emphasise the signal. The resultant 'subtracted' spectra are shown in figure 12. A clear signal is visible for the lower x_E region, but at large x_E, the increased effects of charmed meson production serve to complicate the $K\pi$ mass spectrum. This meant that the production rate could only be measured over a limited x_E range.

The multiplicity could not be extracted from the data using the same procedure as for the vector mesons since the JETSET event sample did not include tensor mesons. The Monte Carlo data generated using HERWIG did contain the $K_2^*(1430)^0$, but it could not be used either in the fits since HERWIG does not correctly simulate the natural widths of resonant states. (The HERWIG sample was used nonetheless to calculate the acceptance.) Instead the data were fitted to a parameterisation made up of signal and background contributions. Two signal shapes were fitted to the peak, a relativistic Breit-Wigner which is the theoretical shape of the state, and a simple Gaussian. These shapes were combined with both parabolic and exponential background functions, yielding four possible fit combinations. The fits were carried out over a mass range from 1.05 up to 1.8 GeV. Initially the mass and width of the signal were allowed to vary and the resulting parameters were found to be consistent with the nominal values for the $K_2^*(1430)^0$ [23]. For example, using a relativistic Breit-Wigner signal and an exponential background the mass and width of the state were determined to be $m_{K_2^*} = 1.434 \pm 0.010$ GeV and $\Gamma_{K_2^*} = 0.104 \pm 0.032$ GeV. For the final fits these two parameters were fixed at the Particle Data Group default values. An example of one of the fits, using a combination of an exponential and a Gaussian is shown in figure 12.

Two further signal measurements were made by fitting the background functions to the side bands of the mass spectra. The overall signal was taken as the mean of the values obtained from the six fits. The deviation from this mean was used as an estimate of the systematic uncertainty in the signal.

Source of systematic	Error on $K_2^*(1430)^0$ rate
Acceptance determination	± 0.048
Signal fitting	± 0.027
Particle identification efficiency	± 0.013
Branching ratio	± 0.005
Total	± 0.057

Table 5: Systematic uncertainties on the $K_2^*(1430)^0$ rate.

The overall efficiency was studied using decays of the $K_2^*(1430)^0$ to $K\pi$ in HERWIG events. In order to estimate the systematic uncertainties, the acceptance for unrelated $K\pi$ track combinations with invariant mass within the fitted mass region was also determined from both JETSET and HERWIG Monte Carlo samples. These combinations have similar kinematics to those from $K_2^*(1430)^0$ decays. The results from these two last samples were in agreement.

To make a direct comparison of the overall acceptance determined using unrelated $K\pi$ combinations with that from $K_2^*(1430)^0$ decays in HERWIG the former was reweighted to take account of the anisotropy of the decay angular distribution in the centre of mass frame of the two track combination. This distribution would be expected to be isotropic for $K_2^*(1430)^0$ decays but biased towards the jet axis for the background combinations. The acceptance for the unrelated track pairs was found to be significantly lower than that measured using $K_2^*(1430)^0$ decays. For this reason the average of the two HERWIG acceptance measurements was used and the difference included as a part of the systematic uncertainty.

The overall multiplicity for $x_E < 0.3$ was determined to be $0.19 \pm 0.04 \pm 0.06$ $K_2^*(1430)^0$ mesons per hadronic Z^0 decay. The main contributions to the systematic error were from the signal and acceptance measurements as outlined above. Other smaller contributions came from $K\pi$ identification efficiency measurements and the $K_2^*(1430)^0 \rightarrow K\pi$ branching ratio. A summary of the systematic errors is given in table 5.

8 Discussion and conclusions

The measurements of $\phi(1020)$ and $K^*(892)^0$ meson production in Z^0 decay reported in this paper represent a significant improvement in precision over those previously published. Table 6 shows the measured production rates together with the values obtained from the JETSET and HERWIG Monte Carlo models. Also listed are the multiplicities obtained from JETSET after certain parameters had been adjusted as described in [4]. For both the vector states, default JETSET and HERWIG predict a significantly larger rate than the measured values. The tuned version of JETSET is however in agreement with the measured $K^*(892)^0$ rate and within two standard deviations of the experimental $\phi(1020)$ multiplicity.

The overall shape of the differential cross sections measured as a function of x_E (figures 8 and 9) are in good agreement with both Monte Carlo models for x_E less than 0.5. The Monte Carlo predictions for the fragmentation functions are significantly different for $x_E > 0.5$. In this region the data for both vector mesons are in somewhat better agreement with HERWIG than with JETSET.

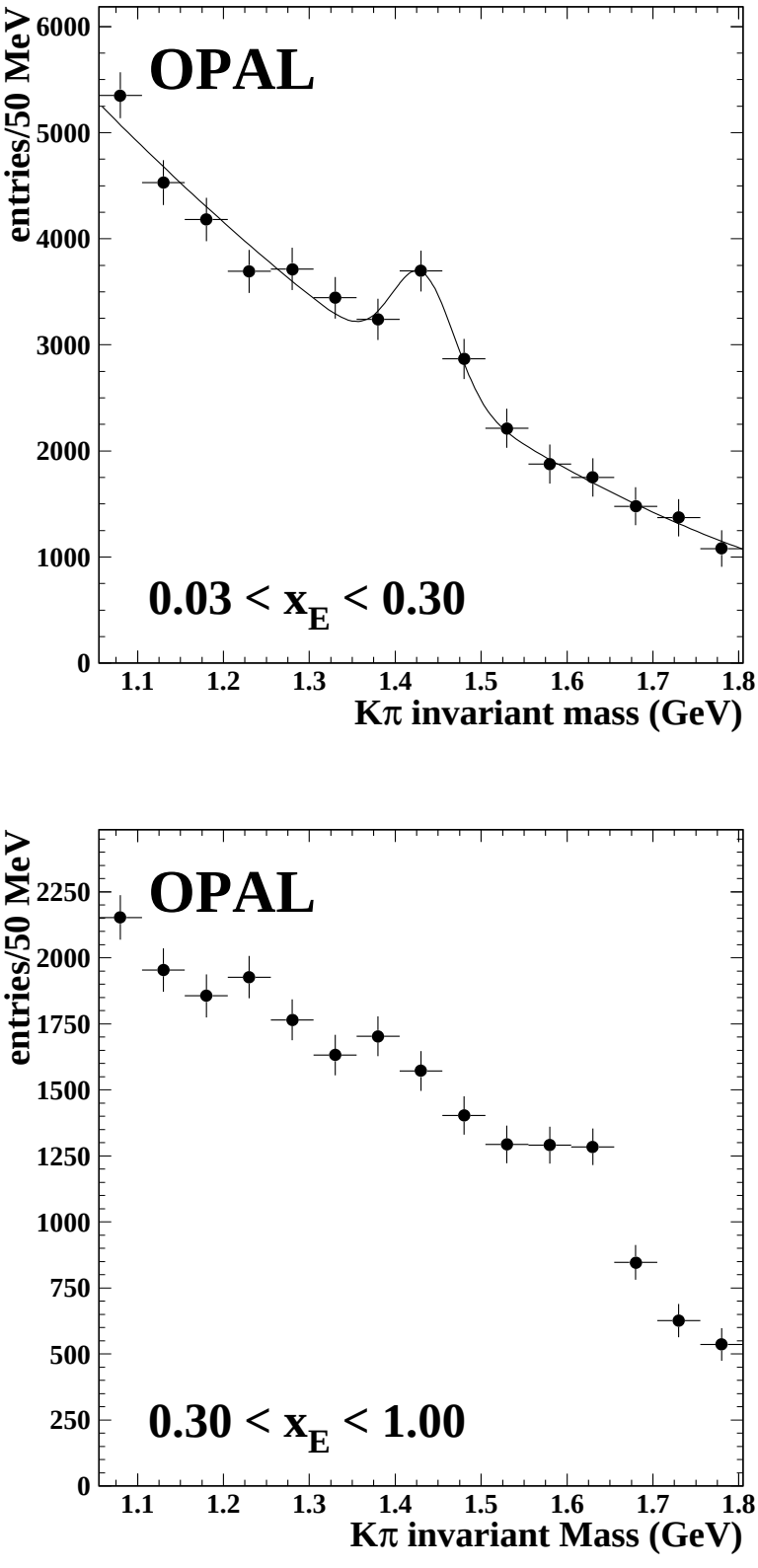

Figure 12: Invariant mass spectra for Kπ combinations around the $K_2^*(1430)^0$ mass.

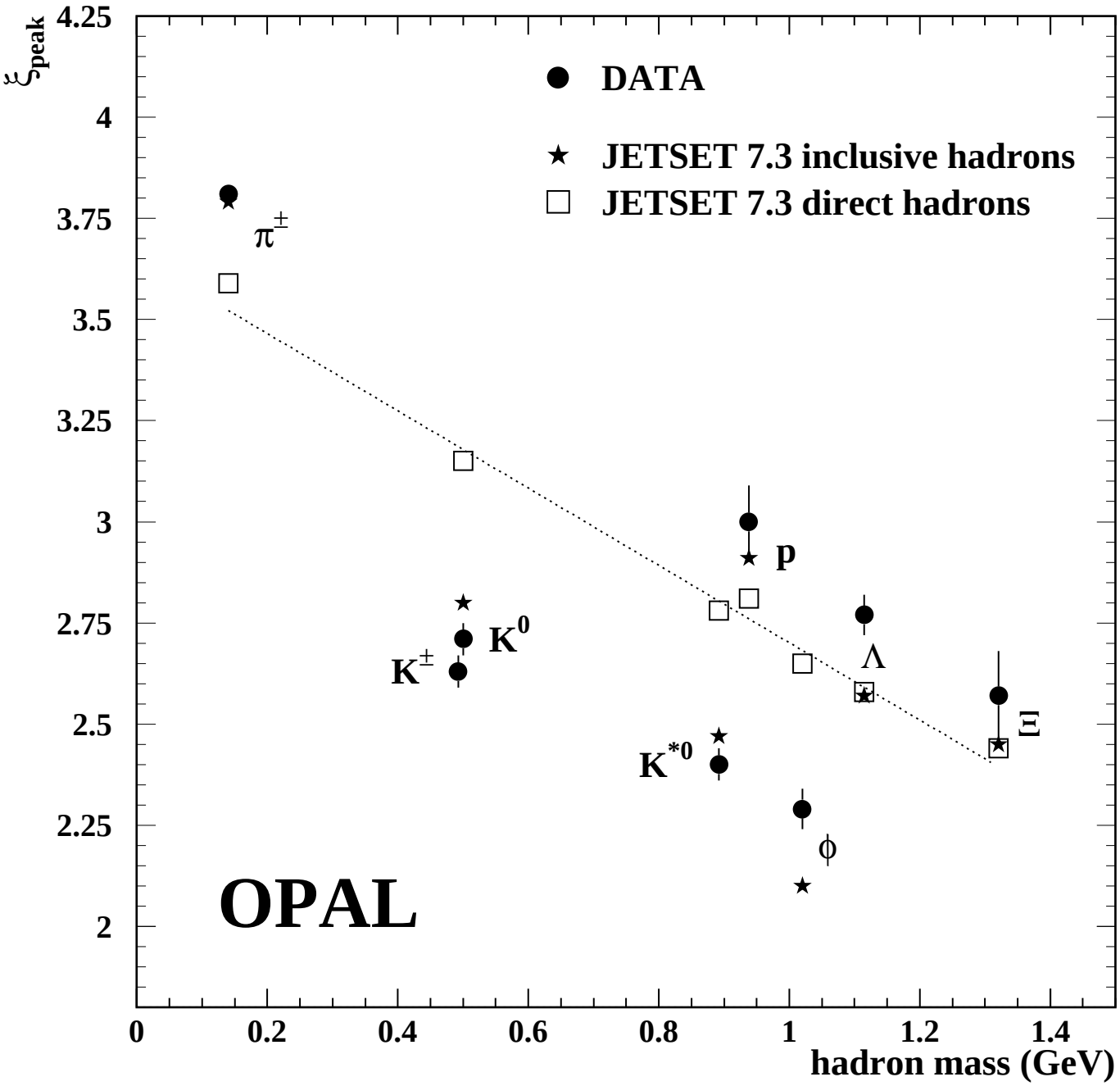

Figure 13: The variation of ξ_{peak} with mass for various hadron states. Measured data points are shown as circles. For JETSET Monte Carlo two points are shown for each particle, the value of ξ_{peak} if inclusive hadrons are considered and that if only those formed directly from a string are used. For kaons in the Monte Carlo one marker represents both the charged and neutral states.

Particle	OPAL data	JETSET default	JETSET tuned	HERWIG
$\phi(1020)$	0.100 ± 0.008	0.191	0.115	0.136
$K^*(892)^0$	0.74 ± 0.04	1.05	0.71	0.87
$K_2^*(1430)^0$	0.19 ± 0.07	–	–	0.11

Table 6: Measured and predicted multiplicities for vector and tensor meson production in Z^0 decay. The values for the $K_2^*(1430)^0$ are over the restricted range, $x_E < 0.3$.

The differential cross sections plotted with respect to the variable $\xi = \ln(1/x_p)$ were found to be well described by a Gaussian shape. The measured peak positions plotted against particle mass are shown in figure 13 along with data from other hadron states [1, 3, 24]. The JETSET Monte Carlo model predicts values of $\xi_{\rm peak}$ which are in broad agreement with the data for all the measured hadrons. A linear decrease in $\xi_{\rm peak}$ as a function of mass is obtained from the Monte Carlo when only hadrons coming directly from the string, rather than from decay of a more massive hadron, are considered, as shown in figure 13. The inclusion of secondary particles from the decay of other hadrons smears out the simple mass dependence, thus producing the pattern observed in the data.

The HERWIG prediction for the $K_2^*(1430)^0$ multiplicity in Z^0 decays is consistent with the measurement. It is likely that the ratio of tensor to vector production rates will be similar for strange and non-strange mesons. A ratio for non-strange mesons of 0.24 ± 0.07 for $x_E > 0.05$ has been measured for the $f_2(1270)$ and the $\rho(770)^0$ in [6]. The ratio for strange particles, $K_2^*(1430)^0$ to $K^*(892)^0$, from our measurements is 0.29 ± 0.10 for $x_E < 0.3$. The two values agree within rather large errors.

Acknowledgements

It is a pleasure to thank the SL Division for the efficient operation of the LEP accelerator, the precise information on the absolute energy, and their continuing close cooperation with our experimental group. In addition to the support staff at our own institutions we are pleased to acknowledge the
Department of Energy, USA,
National Science Foundation, USA,
Particle Physics and Astronomy Research Council, UK,
Natural Sciences and Engineering Research Council, Canada,
Fussefeld Foundation,
Israel Ministry of Science,
Israel Science Foundation, administered by the Israel Academy of Science and Humanities,
Minerva Gesellschaft,
Japanese Ministry of Education, Science and Culture (the Monbusho) and a grant under the Monbusho International Science Research Program,
German Israeli Bi-national Science Foundation (GIF),
Direction des Sciences de la Matière du Commissariat à l'Energie Atomique, France,
Bundesministerium für Forschung und Technologie, Germany,
National Research Council of Canada,
A.P. Sloan Foundation and Junta Nacional de Investigação Científica e Tecnológica, Portugal.

References

[1] R. Akers et al., OPAL Coll.: "The production of neutral kaons in Z^0 decays and their Bose-Einstein correlations", CERN-PPE/95-24;
G. Alexander et al., OPAL Coll.: Phys. Lett. B264 (1991) 467.

[2] D. Buskulic et al., ALEPH Coll.: "Inclusive $\pi^{\pm}$, $K^{\pm}$ and ($p\bar{p}$) Differential Cross-sections at the Z Resonance", CERN-PPE/94-201;
D. Buskulic et al., ALEPH Coll.: Z. Phys. C64 (1994) 361;
D. Buskulic et al., ALEPH Coll.: Phys. Lett. B292 (1992) 210;
O. Adriani et al., L3 Coll.: Phys. Lett. B286 (1992) 403;
B. Adeva et al., L3 Coll.: Phys. Lett. B259 (1991) 199;
M. Acciarri et al., L3 Coll.: Phys. Lett. B328 (1994) 223.;
P. Abreu et al., DELPHI Coll.: Phys. Lett. B275 (1992) 231.

[3] R. Akers et al., OPAL Coll.: Z. Phys. C63 (1994) 181.

[4] P.D. Acton et al., OPAL Coll.: Z. Phys. C56 (1992) 521.

[5] P.D. Acton et al., OPAL Coll.: Phys. Lett. B305 (1993) 407.

[6] P. Abreu et al., DELPHI Coll.: "Production Characteristics of K^0 and Light Meson Resonances in Hadronic Decays of the Z^0", CERN-PPE/94-130.

[7] P. Abreu et al., DELPHI Coll.: Phys. Lett. B298 (1993) 236.

[8] T. Sjöstrand: Comp. Phys. Commun. 39 (1986) 347;
T. Sjöstrand: Comp. Phys. Commun. 43 (1987) 367;
M. Bengtsson and T. Sjöstrand: Nucl. Phys. B289 (1987) 810.

[9] K. Ahmet et al., OPAL Coll.: Nucl. Instr. and Meth. A305 (1991) 275.

[10] P. Allport et al.: Nucl. Instr. and Meth. A324 (1993) 34.

[11] G. Alexander et al., OPAL Coll.: Z. Phys. C52 (1991) 175.

[12] P.D. Acton et al., OPAL Coll.: Z. Phys. C58 (1993) 387;
M.Z. Akrawy et al., OPAL Coll.: Z. Phys. C47 (1990) 505.

[13] J. Allison et. al.: Nucl. Instr. and Meth. A317 (1992) 47.

[14] G. Marchesini and B.R. Webber: Nucl. Phys. B310 (1988) 461;
G. Marchesini et al.: Comp. Phys. Commun. 67 (1992) 465.

[15] M. Hauschild et al.: Nucl. Instr. and Meth. A314 (1992) 74.

[16] P. Abreu et al., DELPHI Coll.: Z. Phys. C63 (1994) 17.

[17] G.D. Lafferty: Z. Phys. C60 (1993) 659.

[18] J.D. Jackson: Nuovo Cim. 34 (1964) 1644.

[19] F. James: CERN Program Library, Ref W515.

[20] G.D. Lafferty and T.R. Wyatt: Nucl. Instr. and Meth. A355 (1995) 541.

[21] Y.L. Dokshitzer, V.A. Khoze and S.I. Troyan : J. Phys. G: Nucl. Part. Phys. 17 (1991) 1481;
Y.L. Dokshitzer, V.A. Khoze and S.I. Troyan : Z. Phys. C55 (1992) 107.

[22] I.N.Bronshtein and K.A.Semendyayev: "Handbook of Mathematics", Van Nostrand Reinhold, 1979.

[23] Particle Data Group: Physical Review D50 (1994) 1173.

[24] P.D. Acton et al., OPAL Coll.: Phys. Lett. B291 (1992) 503.